SCIENCE CHINA Materials ARTICLES

mater.scichina.com link.springer.com

Published online 15 December 2017 | https://doi.org/10.1007/s40843-017-9170-6

Sci China Mater 2018, 61(6): 851–860

SPECIAL ISSUE: Advanced Materials for Photoelectrochemical Cells

Constructing CdS/Cd/doped TiO_2 Z-scheme type visible light photocatalyst for H_2 production

Zhao Zhao[1,2,3,4], Yanbo Xing[1], Haibo Li[1], Pingyun Feng[4*] and Zaicheng Sun[2*]

ABSTRACT **Constructing Z-scheme type photocatalyst is an efficient way to improve the charge separation efficiency and enhance the photocatalytic activity. In this report, the Cd:TiO_2 nanoparticles are prepared *via* the sol-gel route and employed as a starting material. When it was reduced by $NaBH_4$ at 300°C, the surface oxygen vacancies were produced and Cd^{2+} was reduced into metal Cd^0 nanoparticle (denoted as R-Cd:TiO_2). Subsequently, the formed R-Cd:TiO_2 was treated with thiourea in the hydrothermal reaction. Through the decomposition of thiourea, the oxygen vacancies were refilled by S^{2-} from thiourea to form S:TiO_2/TiO_2 (d-TiO_2) and Cd was partially converted into CdS to form CdS/Cd/d-TiO_2 composite. The formed CdS/Cd/d-TiO_2 composite exhibits improved photocatalytic activity. Under visible light irradiation (λ>400 nm), the H_2 production rate of CdS/Cd/d-TiO_2 reaches 119 μmol h^{-1} with 50 mg of photocatalyst without any cocatalyst, which is about 200 and 60 times higher than that of S:TiO_2/TiO_2 (0.57 μmol h^{-1}), CdS (2.03 μmol h^{-1}) and heterojunction CdS/d-TiO_2 (2.17 μmol h^{-1}) materials, respectively. The results illustrate that metal Cd greatly promotes the charge separation efficiency due to the formation of Z-scheme type composite. In addition, the photocatalytic activity in the visible light region was dramatically enhanced due to the contribution of both CdS and d-TiO_2. The method could be easily extended to other wide bandgap semiconductors for constructing visible light responsive Z-scheme type photocatalysts.**

Keywords: Z-scheme, CdS, doped TiO_2, Cd, H_2 production

INTRODUCTION

With increasing demands for alternative sources of fuel, extensive research has focused on the discovery of methods to generate renewable energy from solar energy. Photocatalytic water splitting using inorganic semiconductors is a potentially scalable and economically feasible technology for converting solar energy into hydrogen for fuel cells [1–6]. In recent years, a wide range of inorganic nanomaterials and nanostructures with tunable band gaps have been synthesized and used as photocatalysts for splitting water into hydrogen and oxygen. In addition to generating new materials with narrow band gap, highly efficient charge separation architectures are also desirable to promote the performance of photocatalysts. For example, the design and synthesis of heterojunction Z-scheme architectures have attracted great attention recently [7–11]. This is because the Z-scheme type photocatalytic system, which mimics natural photosynthesis process, retains the reduction capability in the photosystem I (PSI), oxidation capability of photosystem II (PSII) and broad light absorption of both PSI and PSII.

Up to date, three kinds of Z-schemes were developed based on the charge transfer mediator including redox mediators, metal, and direct contact [12–15]. In 2006, Tada and co-workers [16] reported CdS/Au/TiO_2 all solid-state Z-scheme, which employed CdS as PSI photocatalyst, TiO_2 as PSII photocatalyst and Au as electron mediator. After that, different solid state Z-schemes were extensively investigated. Many semiconductors such as, CdS [17,18], AgX [19], g-C_3N_4 [20], Cu_2O [21], doped $SrTiO_3$ [22], $CuGaS_2$ [23] and others were employed as PSI photocatalyst. Most PSII photocatalysts were chosen from TiO_2 [24], ZnO [25], WO_3 [26], Ag_3PO_4 [27], $BiVO_4$

[1] Key Laboratory of Functional Materials Physics and Chemistry of the Ministry of Education, Jilin Normal University, Changchun 130103, China
[2] Beijing Key Lab for Green Catalysis and Separation, Department of Chemistry and Chemical Engineering, College of Environmental and Energy Engineering, Beijing University of Technology, Beijing 100124, China
[3] State Key Laboratory of Electroanalytical Chemistry, Engineering Laboratory for Modern Analytical Techniques, Changchun Institute of Applied Chemistry, Chinese Academy of Sciences, Changchun 130022, China
[4] Department of Chemistry, University of California, Riverside, CA 99025, USA
* Corresponding authors (emails: pingyun.feng@ucr.edu (Feng P); sunzc@bjut.edu.cn (Sun Z))

[28], etc. The common electron mediators used were Au [29], Ag [30], Cu [31] and reduced graphene oxide (RGO) [28,32]. The working principle of Z-scheme is that the light irradiates on both PSI and PSII photocatalysts and then the charge recombination happens between excited electrons from PSII and holes from PSI. As a result, the electrons in conduction band of PSI are available for the reduction reaction and holes in valance band of PSII are ready for oxidation reaction.

It is well known that CdS is a typical visible light photocatalyst, whereas TiO_2 is a UV light responsive photocatalyst due to its large band gap. In the case of the solid-state Z-scheme nanostructure of CdS/Au/TiO_2, Z-scheme works only in the UV light region; it works only as a heterojunction but not Z-Scheme in the visible light region due to no excited electron from TiO_2 in the visible light region. In order to construct visible-light responsive Z-Scheme, both PSI and PSII photocatalysts need to have visible light absorption. One way to achieve this is to use narrow band gap semiconductors such as Ag_3PO_4 or $BiVO_4$ as PSII photocatalysts [27,33]. However, these materials suffer from the low chemical- and photo- stability. Considering the outstanding thermal- and photo-stability of TiO_2, doped TiO_2 can be an excellent candidate as the visible light responsive PSII photocatalyst.

In this report, we develop a new Z-scheme type heterostructure by reducing Cd doped TiO_2 (Cd:TiO_2) nanoparticles (NPs) to form metal Cd NPs on the surface of TiO_2. Subsequently by vulcanizing with thiourea, the Cd NPs are partially converted to CdS leading to the formation of CdS/Cd/doped TiO_2 composite heterostructure. The heterostructure consists of CdS shell and metal Cd core NPs on the surface of TiO_2. Accompanying with this processing, it also promotes the formation of S doped TiO_2 (S:TiO_2/TiO_2). The S:TiO_2/TiO_2 is represented as d-TiO_2. So the formed composite (CdS/Cd/S:TiO_2/TiO_2) is denoted as CdS/Cd/d-TiO_2. Without loading any cocatalysts, the formed CdS/Cd/d-TiO_2 composite exhibits highly efficient H_2 production rates of 227 and 120 μmol h^{-1} under AM1.5 and visible light irradiation, respectively. The photocatalytic activity of CdS/Cd/d-TiO_2 is more than 10 times highter than that of pure CdS, S:TiO_2/TiO_2 and CdS/d-TiO_2 heterojunction in the visible light region (λ > 400 nm).

EXPERIMENTAL SECTION

Materials and chemicals

Titanium(IV) butoxide (TBT, 97%), cadmium acetate dehydrate (>98%), hydrazine hydrate solution (78%–82%), thiourea (>99%), cadmium sulfide powder (>98%), Pluronic® F-127 and $NaBH_4$ (>98%) were purchased from Sigma-Aldrich Company. Concentrated hydrochloric acid (37% by weight), acetic acid (99.7%), ethanol (AR), and methanol (AR) were purchased from Fisher Scientific, and used as received without any further purification.

Preparation of TiO_2 NPs

Mesoporous TiO_2 NPs were prepared through a modified sol-gel method using triblock copolymer as the structure directing agent [34,35]. In a typical reaction, 1.6 g F-127, 3.5 mL TBT, 2.3 mL HAc, and 0.7 mL HCl were dissolved in 30 mL ethanol under magnetic stirring for 60 min, and then was transferred into a 60°C oven to evaporate ethanol for 24 h. The as-prepared gel was calcined at 450°C in air for 4 h using a heating rate of 5°C min^{-1} to remove the surfactant and to obtain ordered mesoporous TiO_2 NPs.

Preparation of Cd-doped TiO_2 NPs (Cd:TiO_2 NPs)

In a typical reaction, 1.6 g F-127, 3.5 mL of TBT (~10 mmol), 2.3 mL HAc, 0.7 mL HCl and a certain amount of $Cd(Ac)_2$ (0.1–1 mmol) were dissolved in 30 mL ethanol under magnetic stirring for 60 min, and then the sol-gel precursor was transferred into a 60°C oven to evaporate ethanol for 24 h. The as-prepared gel was calcined at 450°C in air for 4 h using a heating rate of 5°C min^{-1} to remove the surfactant and to obtain ordered mesoporous TiO_2 NPs.

Preparation of reduced mesoporous Cd/TiO_2 NPs (R-Cd:TiO_2 NPs)

At room temperature, the mesoporous Cd-doped TiO_2 NPs was mixed with $NaBH_4$ at a molar ratio of 2:1 and then grounded for 30 min thoroughly. Then the mixture was transferred into a porcelain boat, and placed in a tubular furnace, heated from room temperature to 300°C under Ar atmosphere at a heating rate of 10°C min^{-1} and then hold for a designed time. After naturally cooling down to room temperature, the final product was simply washed with deionized water and ethanol for several times to remove unreacted $NaBH_4$, and dried at 70°C in electronic oven. The reduced mesoporous TiO_2 NPs (R-TiO_2 NPs) were also prepared as the same procedure by using mesoporous TiO_2 NPs instead of mesoporous Cd-doped TiO_2 NPs.

Preparation of mesoporous CdS/Cd/d-TiO_2 NPs (CdS/Cd/d-TiO_2 NPs)

The reduced Cd-doping mesoporous TiO_2 NPs and

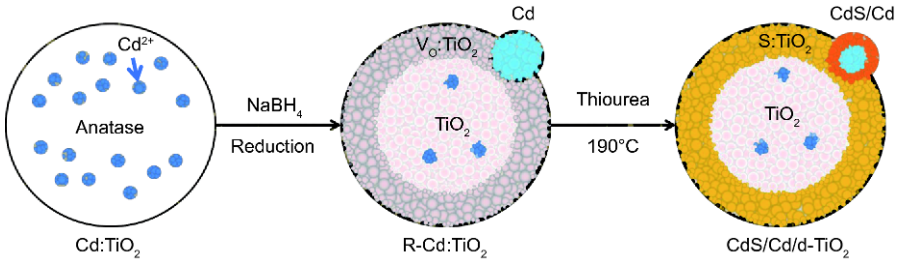

Scheme 1 The synthesis route of CdS/Cd/d-TiO_2 core/shell type heterostructure composite.

thiourea were mixed with a certain molar ratio, and then dissolved in 30 mL hydrazine hydrate under constantly magnetic stirring for 20 min at room temperature. Afterward the solution was sealed into a 20-mL Teflon lined stainless autoclave and heated to 180°C in an electric oven for 24 h, and then naturally cooled to room temperature. The as-prepared precipitate was collected by centrifugation at 5,000 rpm for 15 min, washed with deionized water and ethanol for three times, respectively. Finally, the precipitate was dried in a 70°C electronic oven over 12 h. S doped mesoporous TiO_2 NPs (S:TiO_2 NPs) were also prepared in a similar procedure except for that the reduced mesoporous TiO_2 NPs were used instead of the reduced Cd-doping mesoporous TiO_2 NPs.

Photocatalytic activity measurements

The photocatalytic activities of samples were evaluated by photocatalytic H_2 generation. A photocatalyst (50 mg) without loading noble metal was sealed into 130 mL aqueous solution of 0.35 mol L^{-1} Na_2SO_3 and 0.35 mol L^{-1} Na_2S in the cell with a closed gas circulation system and then magnetically stirred during the whole photocatalytic testing. The visible light source was a 300-W Xe lamp (Beijing Perfectlight Technology Co. Ltd) with an optical filter (UVIRCUT-400, Newport) to cut off the short wavelength part (<400 nm). An AM 1.5 simulated solar power system (Newport) was used as natural light irradiation source. The evolved gases were detected *in situ* by using an online gas chromatograph (SRI 8610C) equipped with a thermal conductivity detector (TCD).

Characterizations

The crystalline structure was recorded by using an X-ray diffractometer (XRD) (Bruker AXS D8 Focus), using Cu Kα radiation (λ=1.54056 Å; 40 kV, 40 mA). Transmission electron microscopy (TEM) images were taken using an FEI Tecnai G2 operated at 200 kV. Scanning electron microscopy (SEM) images were measured on a JEOL JSM 4800F. The UV-vis absorption spectra were recorded on a UV-3101PC UV-vis-NIR scanning spectrophotometer (Shimadzu). X-ray photoelectron spectra (XPS) were obtained on a Thermo Scientific ESCALAB 250 Multitechnique Surface Analysis. The electron paramagnetic resonance (EPR) spectra were recorded at 100K on a Bruker A-200 EPR spectrometer. The specific surface area was calculated using the Brunauer–Emmett–Teller (BET) method from the nitrogen absorption data measured on a Micromeritics ASAP2010 volumetric absorption analyzer at 77 K. The steady-state photoluminescence (PL) spectra measurement was obtained by Horiba Jobin Yvon Fluorolog-3 spectrophotometer with a 150 W ozone-free xenon arc-lamp as the continuous excitation source.

RESULTS AND DISCUSSION

The preparation process of CdS/Cd/d-TiO_2 involves three steps: the formation of Cd:TiO_2, reduction and vulcanization, as shown in Scheme 1. Cd:TiO_2 NPs are synthesized by adding Cd^{2+} into TiO_2 sol-gel precursor in the presence of F127 and then calcined at 450°C. The morphology of Cd:TiO_2 is spherical NPs with a size less than 10 nm as shown in Fig. 1a inset. XRD patterns confirm that both TiO_2 and Cd:TiO_2 are anatase phase (Fig. S1). No characteristic peak of CdO was observed in the XRD patterns even 10 mol% Cd^{2+} was added into TiO_2 sol-gel precursor. The diffraction peak at 25°, attributed to anatase TiO_2 (101), turns weak and broad. According to the Scherrer equation $D=K\gamma/B\cos\theta$, where, D is the size of crystalline domain, K is the shape factor with a typical value of 0.9, γ is the X-ray wavelength, B is the line broadening at half maximum intensity (FWHM), θ is the Bragg angle, the size of Cd:TiO_2 NPs gradually decreases with the increase in the amount of $Cd(OAc)_2$. XPS was employed to probe the element composition and valence state of Cd:TiO_2. Fig. S2 shows Cd 3d, Ti 2p and O 2p peaks at 405, 458 and 532 eV, respectively, which confirm the presence of Cd. High resolution XPS spectra of Cd 3d exhibit two peaks at 405.6 and 412.3 eV indicating the Cd is in Cd^{2+} state. Element mapping images (Fig. S3) show

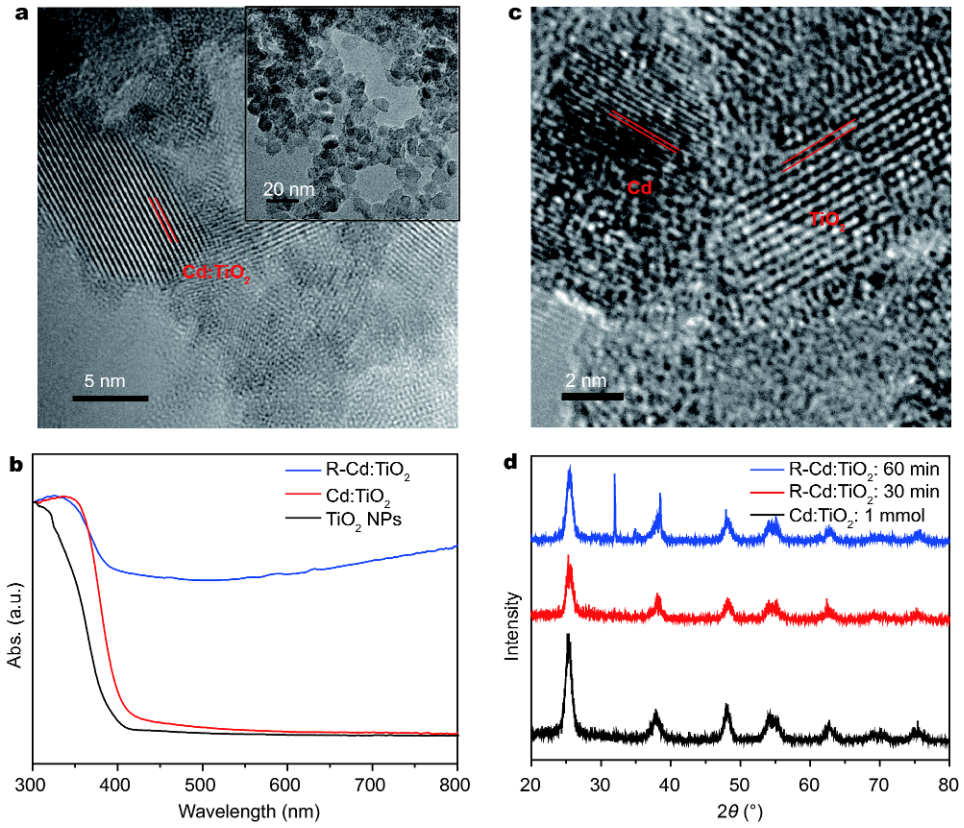

Figure 1 Characterization of $Cd:TiO_2$ and reduced $Cd:TiO_2$. (a) HR-TEM graph of $Cd:TiO_2$ (inset is a low magnitude TEM image of $Cd:TiO_2$). (b) UV-vis spectra of TiO_2 NPs, $Cd:TiO_2$ and $Cd:TiO_2$ after $NaBH_4$ treatment for 30 min (R-$Cd:TiO_2$). (c) HR-TEM of R-$Cd:TiO_2$ NPs; (d) XRD patterns of $Cd:TiO_2$, R-$Cd:TiO_2$ treated for 30 and 60 min.

that Cd, Ti and O are uniformly dispersed in the whole sample. High resolution TEM (HR-TEM) photography of $Cd:TiO_2$ (Fig. 1a) exhibits clear lattice fringes of 0.35 nm corresponding to the (110) of anatase TiO_2 crystal. It further confirms that the as-prepared $Cd:TiO_2$ has crystalline anatase phase. After doping with Cd, the optical band edge has a clear red-shift from 387 to 409 nm (Fig. 1b). That moves the band gap of $Cd:TiO_2$ to 3.0 eV *vs.* 3.2 eV for TiO_2. The doping concentration of Cd can be tuned by tuning the amount of $Cd(OAc)_2$.

Furthermore, $Cd:TiO_2$ NPs were mixed with $NaBH_4$ by grounding and then the mixture was placed at 350°C for 30 or 60 min in flowing argon at atmospheric pressure. The surface (shell) of the $Cd:TiO_2$ NPs was reduced during the $NaBH_4$ decomposition to form metal Cd NPs and the reduced TiO_2 with oxygen vacancies (denoted as R-$Cd:TiO_2$) as shown in Scheme 1. Fig. 1c displays the HR-TEM images of R-$Cd:TiO_2$. It clearly illustrates that the metal Cd NPs with 0.14 nm of lattice fringe located besides the TiO_2 NPs with 0.35 nm of lattice fringe. Amorphous TiO_2 shell is observed surrounding the R-Cd:TiO_2 NPs (Fig. 1c). After $NaBH_4$ treatment, the optical band edge of R-$Cd:TiO_2$ further shifts towards visible light (~460 nm) and another broad absorption band appears in the visible light region due to the introducing of oxygen vacancies (Fig. 1b), which matches well with our previous reported result [36]. All these results confirm that the $NaBH_4$ treatment not only transferred the surface Cd^{2+} into Cd metal NP, but also promoted the formation of the reduced TiO_2 NPs shell with surface oxygen vacancies. Fig. 1d exhibits the XRD patterns of $Cd:TiO_2$ and R-$Cd:TiO_2$ with different treatment time. After 30 min treatment, there is a very weak peak appear at 32°, which is characteristic diffraction peak of metal Cd NPs. The peak turns stronger when the treatment time prolongs to 60 min. It indicates the $NaBH_4$ treatment could reduce Cd^{2+} in $Cd:TiO_2$ into Cd metal NPs. Particle size of R-$Cd:TiO_2$ calculated by Scherrer formula decreases from 13.24 to 12.04 nm, which is well consistent with that of crystal size observed by TEM images.

Furthermore, R-$Cd:TiO_2$ was treated with thiourea under hydrothermal condition, which has two purposes:

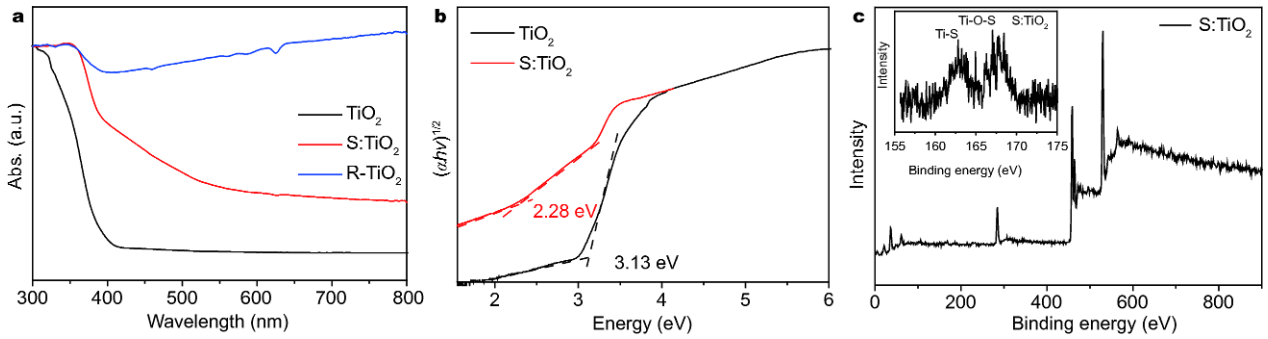

Figure 2 Optical properties and XRD of TiO_2 and S:TiO_2. (a) Diffuse reflectance UV-vis spectra of TiO_2, R:TiO_2 and S:TiO_2 represented as d-TiO_2(S:TiO_2/TiO_2). (b) Transformed Kubelka-Munk function *vs.* photon energy plot of TiO_2 and S:TiO_2. (c) Full XPS spectra of S:TiO_2 (inset is the high resolution S 2p XPS spectra).

(i) S^{2-} refills back to oxygen vacancies of R-Cd:TiO_2 to form core shell structure of S:TiO_2/TiO_2; (ii) metal Cd NPs in the out-shell are vulcanized and form CdS or CdS/Cd nanostructure depending on the amount of thiourea. In order to confirm that S^{2-} can refill the site of oxygen vacancy, R-TiO_2 was prepared by $NaBH_4$ treatment of TiO_2 as the same route as R-Cd:TiO_2 then treated with thiourea. Fig. 2a shows the UV-vis spectra of TiO_2, R-TiO_2 and S:TiO_2 NPs. After $NaBH_4$ treatment, TiO_2 is reduced to form R-TiO_2 with surface oxygen vacancies. Its UV-vis spectrum shows strong broad light absorption in the visible light region. After thiourea treatment, a band tail in the range of 410–520 nm appears in the UV-vis spectrum. The band tail can be attributed to the formation of S doped TiO_2 (S:TiO_2) which exhibits narrower band gap of 2.28 eV from transformed Kubelka-Munk function *vs.* photon energy plot (Fig. 2b). This result also confirms that S:TiO_2 has broad absorption in the visible light region. In addition, the absorption decreasing in the IR region for the S:TiO_2 demonstrates the decrease of oxygen vacancies. Furthermore, XPS spectra of S:TiO_2 (Fig. 2c) also display a peak at ~165 eV, which corresponds to the S 2p signal, which confirms the presence of S^{2-} in the thiourea treated TiO_2 sample. The valence band XPS spectra of TiO_2 and S:TiO_2 (Fig. S4) show that the band edge of S:TiO_2 shifts to low binding energy, indicating the valence band of S:TiO_2/TiO_2 shift upwards due to S 2p orbital has lower binding energy [37].

Fig. 3a displays the XRD patterns of R-Cd:TiO_2 hydrothermally treated with different amounts of thiourea. When the molar ratio of Cd/thiourea is less than 1/1, a new series of XRD peaks are observed at 26.6°, 28.3°, 43.8°, and 51.9°, which can be assigned to wurtzite type CdS (PDF# 77-2306). The diffraction peak at 32° still exists and peak intensity decreases, indicating that metal Cd NPs and CdS co-exist in the sample. When excess amount of thiourea (Cd/S=1/10) was added into the reaction, the characteristic peak of metal Cd disappears and only CdS characteristic diffraction peaks are observed, indicating that the metal Cd can be fully converted into CdS in the hydrothermal reaction.

HR-TEM image (Fig. 3b) illustrates three kinds of NPs with lattice fringe of 0.35, 0.14 and 0.32 nm, respectively, corresponding to (101) of TiO_2, (004) of Cd and (101) of CdS, respectively. Metal Cd was sandwiched between CdS and TiO_2 NP. Fig. 3c shows the UV-vis spectra of thiourea treated R-Cd:TiO_2 with different amounts of thiourea. With the formation of CdS, another absorption band in the 400–550 nm region appears. With pure CdS as a reference, this band can be assigned to the absorption of CdS in the composite. It should be noted that the absorption band shape of Cd/S=5/1 is closer to that of S:TiO_2/TiO_2 (Figs 2a and 3c) than other samples. It may imply that the S^{2-} produced from thiourea refills oxygen vacancies to form S:TiO_2 prior to reacting with Cd to produce CdS. Excess amount of thiourea results in the formation of CdS/d-TiO_2 heterojunction due to that the metal Cd is fully transferred into CdS. Fig. 3d shows the high resolution Cd XPS spectra of Cd:TiO_2, R-Cd:TiO_2 and CdS/Cd/d-TiO_2. Two peaks at 405.6 and 412.3 eV are contributed from Cd $3d_{5/2}$ and $3d_{3/2}$, respectively. In the case of R-Cd:TiO_2, these peaks shift toward low binding energy 404.8 and 411.5 eV due to the formation of metal Cd. After thiourea treatment, these peaks shift back to high binding energy 405.1 and 411.9 eV, respectively. Those results indicate that partial Cd^0 was converted into Cd^{2+} in the treatment, which matches with our results and explanation. We also checked the EPR spectra to understand the changes of the oxygen vacancy in the treatment. EPR spectra (Fig. S5) clearly show that the TiO_2 and CdS

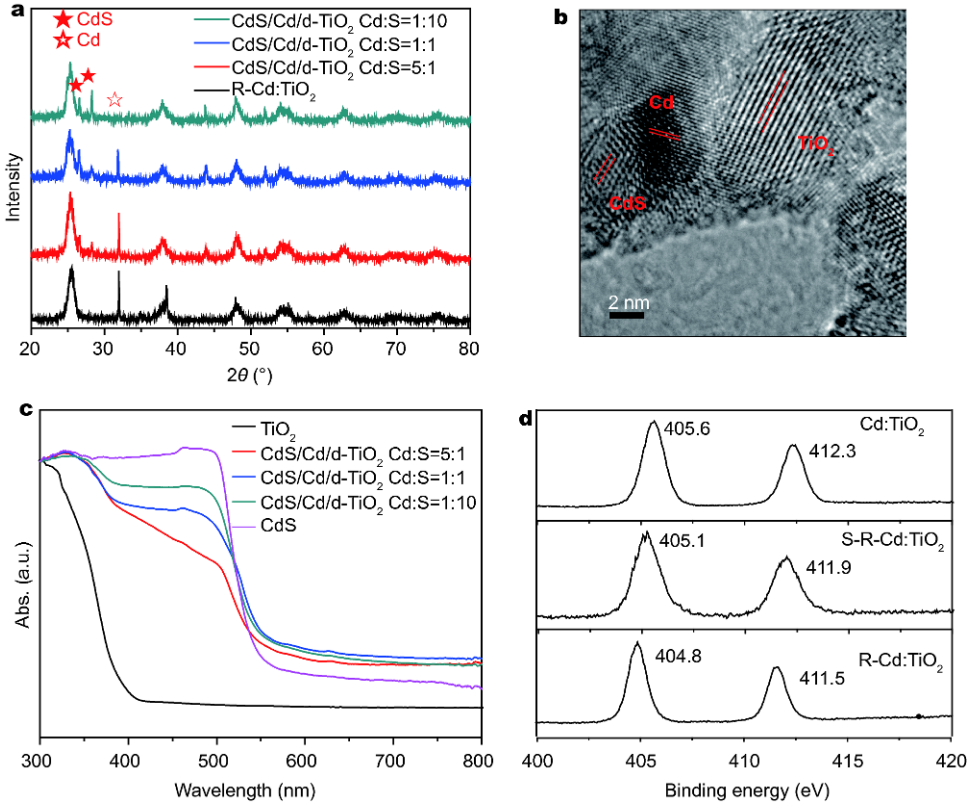

Figure 3 (a) XRD patterns of R-Cd:TiO_2 and hydrothermally treated R-Cd:TiO_2 with different amounts of thiourea. (b) HR-TEM image of CdS/Cd/d-TiO_2. (c) UV-vis spectra of TiO_2, CdS, and CdS/Cd/d-TiO_2 obtained with different amounts of thiourea treatment. (d) High resolution Cd XPS of the as-prepared Cd:TiO_2, R-Cd:TiO_2 and CdS/Cd/d-TiO_2 NPs.

did not display vacancy signal at 3,418 Gauss. The samples treated with $NaBH_4$ exhibit strong EPR signal, which confirms the presence of oxygen vacancies. Although the EPR signal decreases in the sample treated with thiourea (CdS/Cd/d-TiO_2), the oxygen vacancies still exist in the sample inside.

In general, solid state Z-scheme such as CdS/Au/TiO_2 works well in the UV light region, because the excited charge can only be produced in the UV light region for at least one component such as the TiO_2 photocatalyst. It is prerequisite to have both PSI and PSII photocatalysts respond to visible light in order to constructing Z-scheme nanostructure working in visible light region. Here the synthesized heteronanostructures were used as PSII photocatalysts. Photocatalytic H_2 production activities were evaluated under both AM 1.5 and visible light ($\lambda >$ 400 nm) irradiation by using Na_2SO_3-Na_2S buffer solution as the sacrificial reagent to quench the photo-induced holes. Firstly, photocatalytic H_2 evolution rates of control samples like TiO_2, R-TiO_2 and R-Cd:TiO_2 without loading cocatalyst under AM 1.5 (1 Sun) irradiation were studied and the results were listed in Fig. S6. The as-prepared TiO_2 NPs showed the H_2 evolution rate of about 24 μmol h^{-1} for 50 mg of photocatalyst. After $NaBH_4$ treatment, oxygen vacancies were introduced onto the surface of TiO_2 NPs (R-TiO_2). The photocatalytic activity of R-TiO_2 was improved to 50.3 μmol h^{-1}, which doubled the H_2 evolution rate of the original TiO_2 NPs. The H_2 evolution rate of Cd:TiO_2 sample exhibited similar improvement as that of R-TiO_2. These results agree well with our previous reports [36]. Further sulfurization of R-TiO_2 led to the formation of S:TiO_2/TiO_2, whose photocatalytic activity was close to that of R-TiO_2 without obvious improvement. Fig. S7 illustrates the visible light photocatalytic activities of these samples. The study confirms that TiO_2 has almost negligible photocatalytic activity due to its large band gap. Although R-TiO_2 and S:TiO_2/TiO_2 (Fig. 4b) show clear visible light absorption, their photocatalytic activities are relatively weak in the visible light region [36].

The H_2 production rates of S:TiO_2/TiO_2, CdS, CdS/Cd/d-TiO_2 and CdS/d-TiO_2 under the AM 1.5 irradiation (1

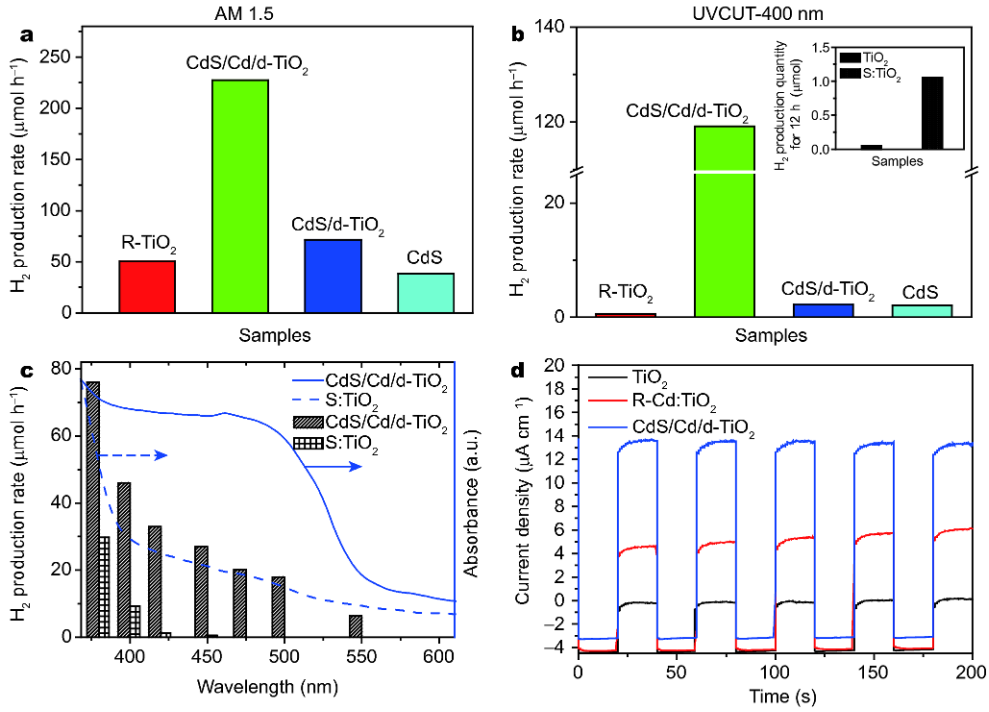

Figure 4 H_2 evolution rate of S:TiO_2, CdS, CdS/Cd/d-TiO_2 and CdS/TiO_2 under AM 1.5 (a) and visible light (λ>400 nm) (b) irradiation in the 0.35 mol L^{-1} Na_2SO_3-0.35 mol L^{-1} Na_2S aqueous solution. The inset of (b) is the H_2 production rate of TiO_2 and S:TiO_2 under visible light. (c) H_2 production dependence of CdS/Cd/d-TiO_2 and CdS/TiO_2 on the wavelength under different band pass, the curves are the UV-vis spectra of S:TiO_2 (dash) and CdS/Cd/d-TiO_2 (solid). (d) Transient photocurrent responses of TiO_2, R-Cd:TiO_2 and CdS/Cd/d-TiO_2.

Sun) are summarized in the Fig. 4a. The H_2 evolution rates of S:TiO_2/TiO_2 and CdS were 50.3 and 38.4 μmol h^{-1}, respectively, for 50 mg photocatalyst without Pt cocatalyst. R-Cd:TiO_2 displayed slightly enhanced photocatalytic activity (57 μmol h^{-1}) in comparison with R-TiO_2. This improvement could be caused by the formation of metal Cd NPs, which promoted the charge separation and functioned as a cocatalyst. CdS/Cd/d-TiO_2 composite treated under Cd:S=1:1 condition exhibited much higher photocatalytic H_2 evolution rate (227 μmol h^{-1}) than that of other samples studied here, which is about 4–5 times better than that of S:TiO_2 and CdS. With excess amount of thiourea used in the sulfuration reaction (Cd:S=1:10), metal Cd was fully converted into CdS leading to the formation of CdS/d-TiO_2 heterojunction, no longer a Z-scheme, in which photogenerated electrons transferred from CdS to TiO_2. In comparison with other single component CdS or d-TiO_2, heterojunction CdS/d-TiO_2 showed improved photocatalytic activities because the heterojunction structural feature can improve the charge separation. The photocatalytic activities of CdS/d-TiO_2 is two-fold higher than that of CdS or S:TiO_2/TiO_2. Our studies show that CdS/Cd/d-TiO_2 possessed even better photocatalytic activity than that of heterojunction due to the existence of metal Cd, although the samples have quite similar absorption capability. Fig. 4b illustrates the photocatalytic H_2 production rates of S:TiO_2/TiO_2, CdS, CdS/Cd/d-TiO_2 and CdS/d-TiO_2 under visible light irradiation. Both S:TiO_2/TiO_2 and CdS exhibit relatively weak photocatalytic activity of 0.57 and 2.03 μmol h^{-1} without loading Pt cocatalyst. The CdS/d-TiO_2 heterojunction with less than 10% of CdS displays 2.17 μmol h^{-1} of H_2 production rate for 50 mg photocatalyst. The CdS/Cd/d-TiO_2 exhibits significant enhanced photocatalytic activity. The H_2 production rate reaches 119 μmol h^{-1}, which is near 200 and ~60 times higher than d-TiO_2 and CdS/d-TiO_2 due to the existence of metal Cd NPs. These results indicate that metal Cd greatly promote the charge separation and the photocatalytic performance due to the formation of Z-scheme type photocatalytic system.

To better understand the significant enhancement, the dependence of H_2 production rate on the irradiation wavelength with ~20 nm band-width is shown in Fig. 4c. Although S:TiO_2/TiO_2 has absorption in the visible light region, its H_2 production rate is quite low and almost zero

after 450 nm. The H_2 production rates studied with different wavelengths also decreased dramatically in the visible light region for CdS/d-TiO_2, due to the content of CdS is far below 10 wt% (Fig. S8). In the case of CdS/Cd/d-TiO_2, its absorption curve is close to the absorption curve of CdS in the visible light region. However, the H_2 production rate continuously decreases in the visible light region, the trend of H_2 production rate for CdS/Cd/d-TiO_2 matches well with that of S:TiO_2/TiO_2. That implies that the absorption capability of S:TiO_2/TiO_2 is the restriction factor in the CdS/Cd/d-TiO_2 photocatalyst. Although both CdS/Cd/d-TiO_2 and CdS/d-TiO_2 have similar light absorption, the H_2 production rate of the former is much higher than that of the latter, indicating that the charge separation efficiency of CdS/Cd/d-TiO_2 is much higher than that of CdS/d-TiO_2. This result implies that the formation of Z-scheme structural configuration in the CdS/Cd/d-TiO_2 could have played a pivotal role in the enhancement of the material's photocatalytic activity. PL spectra of S:TiO_2/TiO_2, CdS, CdS/Cd/d-TiO_2 and CdS/d-TiO_2 are shown in Fig. S9. The PL emission was quenched by the formation of CdS/Cd/d-TiO_2 and CdS/d-TiO_2, indicating the charge separation efficiency in the heterostructure is better than that in single component. In addition, only CdS emission was quenched in the CdS/d-TiO_2 heterojunction. Both emissions from TiO_2 and CdS are quenched in the case of CdS/Cd/d-TiO_2 indicating that it has better charge separation efficiency than that of CdS/d-TiO_2. Furthermore, the photoelectrochemical cell was constructed to investigate the transient photocurrent density (Fig. 4d). Comparing with TiO_2 and R-Cd:TiO_2, the CdS/Cd/d-TiO_2 exhibits the highest photocurrent density, which matches well with photocatalytic H_2 production results.

According to the above results, we propose a Z-scheme working mechanism for the CdS/Cd/d-TiO_2 composite photocatalyst (Fig. 5). CdS/Cd/d-TiO_2 exhibits broad visible light absorption due to coexistence of d-TiO_2 and CdS. Under visible light irradiation, both d-TiO_2 and CdS can produce excited charges. The excited electron from d-TiO_2 can recombine with the hole from CdS through the metal Cd. The more reductive electron from CdS and oxidative hole from d-TiO_2 were left in the composite photocatalyst for oxidation and reduction reactions. This greatly enhanced the charge separation efficiency of the system. The composite exhibits much better photocatalytic activity compared with any single component.

CONCLUSIONS

In summary, starting from Cd:TiO_2 through reduction and sulfuration, a novel solid state Z-scheme configuration based on CdS/Cd/d-TiO_2 composite was obtained. Both CdS and d-TiO_2 showed the visible light responsive absorption properties. With the formed Cd metal NPs in the system acting as electron transfer mediator, the composite showed impressive photocatalytic activity in the visible light region. Through series systematic studies, the formed heteronanostructured material was thoroughly understood and well characterized. A working mechanism of the formed Z-scheme was proposed. The reported method is innovative and could be easily extended to other materials for the construction of solid state Z-scheme. This could pave the way toward the search for efficient photocatalytic materials in visible light spectrum.

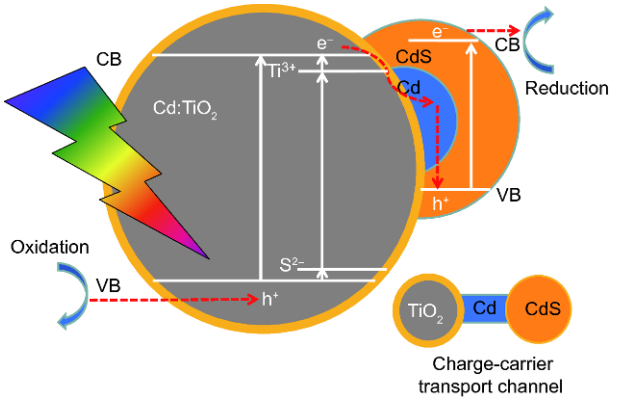

Figure 5 The proposed work mechanism of CdS/Cd/d-TiO_2 composites.

Received 18 October 2017; accepted 27 November 2017; published online 15 December 2017

1 Osterloh FE. Inorganic nanostructures for photoelectrochemical and photocatalytic water splitting. Chem Soc Rev, 2013, 42: 2294–2320
2 Ran J, Zhang J, Yu J, *et al.* Earth-abundant cocatalysts for semiconductor-based photocatalytic water splitting. Chem Soc Rev, 2014, 43: 7787–7812
3 Navarro Yerga RM, Alvarez Galván MC, del Valle F, *et al.* Water splitting on semiconductor catalysts under visible-light irradiation. ChemSusChem, 2009, 2: 471–485
4 Maeda K, Domen K. Photocatalytic water splitting: recent progress and future challenges. J Phys Chem Lett, 2010, 1: 2655–2661
5 Ma XC, Dai Y, Yu L, *et al.* Energy transfer in plasmonic photocatalytic composites. Light Sci Appl, 2016, 5: e16017
6 Shi R, Cao Y, Bao Y, *et al.* Self-assembled Au/CdSe nanocrystal clusters for plasmon-mediated photocatalytic hydrogen evolution. Adv Mater, 2017, 29: 1700803
7 Rao PM, Cai L, Liu C, *et al.* Simultaneously efficient light absorption and charge separation in WO_3/$BiVO_4$ core/shell nanowire photoanode for photoelectrochemical water oxidation. Nano Lett, 2014, 14: 1099–1105

8 Wang H, Zhang L, Chen Z, *et al.* Semiconductor heterojunction photocatalysts: design, construction, and photocatalytic performances. Chem Soc Rev, 2014, 43: 5234–5244
9 Moniz SJA, Shevlin SA, Martin DJ, *et al.* Visible-light driven heterojunction photocatalysts for water splitting—a critical review. Energ Environ Sci, 2015, 8: 731–759
10 Zhang J, Zhang M, Sun RQ, *et al.* A facile band alignment of polymeric carbon nitride semiconductors to construct isotype heterojunctions. Angew Chem, 2012, 124: 10292–10296
11 Chen S, Qi Y, Hisatomi T, *et al.* Efficient visible-light-driven Z-scheme overall water splitting using a $MgTa_2O_{6-x}N_y$/TaON heterostructure photocatalyst for H_2 evolution. Angew Chem, 2015, 127: 8618–8621
12 Maeda K. Z-scheme water splitting using two different semiconductor photocatalysts. ACS Catal, 2013, 3: 1486–1503
13 Zhou P, Yu J, Jaroniec M. All-solid-state Z-scheme photocatalytic systems. Adv Mater, 2014, 26: 4920–4935
14 Li H, Tu W, Zhou Y, *et al.* Z-scheme photocatalytic systems for promoting photocatalytic performance: recent progress and future challenges. Adv Sci, 2016, 3: 1500389
15 Wang X, Liu G, Wang L, *et al.* ZnO-CdS@Cd heterostructure for effective photocatalytic hydrogen generation. Adv Energ Mater, 2012, 2: 42–46
16 Tada H, Mitsui T, Kiyonaga T, *et al.* All-solid-state Z-scheme in CdS–Au–TiO_2 three-component nanojunction system. Nat Mater, 2006, 5: 782–786
17 Jin J, Yu J, Guo D, *et al.* A hierarchical Z-scheme CdS-WO_3 photocatalyst with enhanced CO_2 reduction activity. Small, 2015, 11: 5262–5271
18 Yu ZB, Xie YP, Liu G, *et al.* Self-assembled CdS/Au/ZnO heterostructure induced by surface polar charges for efficient photocatalytic hydrogen evolution. J Mater Chem A, 2013, 1: 2773–2776
19 Ye L, Liu J, Gong C, *et al.* Two different roles of metallic Ag on Ag/AgX/BiOX (X = Cl, Br) visible light photocatalysts: surface plasmon resonance and Z-scheme bridge. ACS Catal, 2012, 2: 1677–1683
20 Zheng D, Pang C, Wang X. The function-led design of Z-scheme photocatalytic systems based on hollow carbon nitride semiconductors. Chem Commun, 2015, 51: 17467–17470
21 Wang JC, Zhang L, Fang WX, *et al.* Enhanced photoreduction CO_2 activity over Direct Z-Scheme α-Fe_2O_3/Cu_2O heterostructures under visible light irradiation. ACS Appl Mater Interfaces, 2015, 7: 8631–8639
22 Wang Q, Hisatomi T, Ma SSK, *et al.* Core/shell structured La- and Rh-codoped $SrTiO_3$ as a hydrogen evolution photocatalyst in Z-scheme overall water splitting under visible light irradiation. Chem Mater, 2014, 26: 4144–4150
23 Iwashina K, Iwase A, Ng YH, *et al.* Z-schematic water splitting into H_2 and O_2 using metal sulfide as a hydrogen-evolving photocatalyst and reduced graphene oxide as a solid-state electron mediator. J Am Chem Soc, 2015, 137: 604–607
24 Ma K, Yehezkeli O, Domaille DW, *et al.* Enhanced hydrogen production from DNA-assembled Z-scheme TiO_2-CdS photocatalyst systems. Angew Chem Int Ed, 2015, 54: 11490–11494
25 Si H, Kang Z, Liao Q, *et al.* Design and tailoring of patterned ZnO nanostructures for energy conversion applications. Sci China Mater, 2017, 60: 793–810
26 Liu Z, Zhao ZG, Miyauchi M. Efficient visible light active $CaFe_2O_4$/WO_3 based composite photocatalysts: effect of interfacial modification. J Phys Chem C, 2009, 113: 17132–17137
27 Chen X, Huang X, Yi Z. Enhanced ethylene photodegradation performance of g-C_3N_4-Ag_3PO_4 composites with direct Z-scheme configuration. Chem Eur J, 2014, 20: 17590–17596
28 Iwase A, Ng YH, Ishiguro Y, *et al.* Reduced graphene oxide as a solid-state electron mediator in Z-scheme photocatalytic water splitting under visible light. J Am Chem Soc, 2011, 133: 11054–11057
29 Li W, Feng C, Dai S, *et al.* Fabrication of sulfur-doped g-C_3N_4/Au/CdS Z-scheme photocatalyst to improve the photocatalytic performance under visible light. Appl Catal B-Environ, 2015, 168-169: 465–471
30 Xie K, Wu Q, Wang Y, *et al.* Electrochemical construction of Z-scheme type CdS–Ag–TiO_2 nanotube arrays with enhanced photocatalytic activity. Electrochem Commun, 2011, 13: 1469–1472
31 Li H, Yu H, Quan X, *et al.* Uncovering the key role of the Fermi level of the electron mediator in a Z-Scheme photocatalyst by detecting the charge transfer process of WO_3-metal-gC_3N_4 (metal = Cu, Ag, Au). ACS Appl Mater Interfaces, 2016, 8: 2111–2119
32 Li P, Zhou Y, Li H, *et al.* All-solid-state Z-scheme system arrays of $Fe_2V_4O_{13}$/RGO/CdS for visible light-driving photocatalytic CO_2 reduction into renewable hydrocarbon fuel. Chem Commun, 2015, 51: 800–803
33 Jia Q, Iwase A, Kudo A. $BiVO_4$–Ru/$SrTiO_3$:Rh composite Z-scheme photocatalyst for solar water splitting. Chem Sci, 2014, 5: 1513–1519
34 Ismail AA, Al-Sayari SA, Bahnemann DW. Photodeposition of precious metals onto mesoporous TiO_2 nanocrystals with enhanced their photocatalytic activity for methanol oxidation. Catal Today, 2013, 209: 2–7
35 Fan J, Boettcher SW, Stucky GD. Nanoparticle assembly of ordered multicomponent mesostructured metal oxides *via* a versatile sol–gel process. Chem Mater, 2006, 18: 6391–6396
36 Tan H, Zhao Z, Niu M, *et al.* A facile and versatile method for preparation of colored TiO_2 with enhanced solar-driven photocatalytic activity. Nanoscale, 2014, 6: 10216–10223
37 Chen X, Burda C. The electronic origin of the visible-light absorption properties of C-, N- and S-doped TiO_2 nanomaterials. J Am Chem Soc, 2008, 130: 5018–5019

Acknowledgements Sun Z thanks the financial support from the National Natural Science Foundation of China (21671011), Beijing High Talent Program, Beijing Natural Science Foundation (KZ201710005002). The authors thank China Postdoctoral Science Foundation, Beijing Postdoctoral Research Foundation, and Dongguan Program for International S&T Cooperation. Zhao Z thanks the support from China Scholarship Council. This research was also supported by the National Science Foundation (DMR-1506661, Feng P).

Author contributions Zhao Z designed and engineered the samples; Zhao Z, Xing Y and Li H performed the experiments. Zhao Z, Sun Z and Feng P wrote the paper. All authors contributed to the general discussion.

Conflict of interest The authors declare that they have no conflict of interest.

Supplementary information Experimental details are available in the online version of the paper.

Zhao Zhao received his PhD degree from Changchun Institute of Optics, Fine Mechanics and Physics, Chinese Academy of Sciences, Changchun, China. He is currently a lecturer in the Key Laboratory of Functional Materials Physics and Chemistry of the Ministry of Education, Jilin Normal University. His main research area includes photocatalyst based on inorganic semiconductors.

Zaicheng Sun is a professor of Beijing Key Lab for Green Catalysis and Separation, Department of Chemistry and Chemical Engineering, College of Environmental and Energy Engineering, Beijing University of Technology, Beijing. China. His research interests are mainly on the photocatalytic nano materials for water splitting, H_2 production, and self-cleaning optical coating, fluorescent carbon dots for theragnostics.

Pingyun Feng is a professor of the Department of Chemistry, University of California, Riverside, CA, USA. She received her PhD degree from the Department of Chemistry, University of California, Santa Barbara. Her research interest centers on the development of synthetic methodologies to prepare novel materials for energy conversion and storage. These materials integrate uniform porosity, high surface area, semi conductivity, optical property, photocatalytic, acid- or base-catalytic properties and have a variety of applications.

构建高效可见光区分解水制氢的Z型CdS/Cd/掺杂TiO_2光催化体系

赵钊[1,2,3,4], 邢艳波[1], 李海波[1], 冯萍云[4*], 孙再成[2*]

摘要 构建Z型光催化体系是提高光生电荷分离效率和光催化活性的一种有效途径. 本文通过溶胶凝胶方法制备了Cd掺杂的TiO_2纳米颗粒, 并通过一步$NaBH_4$固相热还原的方式在材料表面可控地引入氧空位(V_O), 同时掺入的Cd^{2+}可被还原为金属Cd^0纳米粒子(即R-Cd:TiO_2). 进一步将获得的R-Cd:TiO_2材料与硫脲热水反应, 材料表面的V_O可被S^{2-}替代, 同时部分金属Cd^0硫化, 从而获得CdS/Cd/d-TiO_2 Z型光催化复合材料. 研究结果表明该Z型光催化复合材料具有优异的模拟太阳光及可见光区光催化活性和稳定性. 通过实验分析证明构建这种全固态金属-无机半导体Z型光催化复合材料, 金属介质层显著促进了光生电荷的分离与迁移; 此外, 由于CdS和d-TiO_2在可见光区的光吸收作用, 该CdS/Cd/d-TiO_2 Z型光催化复合材料在可见光区的光催化活性获得了显著增强.

